Article

Polyvinylpyrrolidone-Capped Copper Oxide Nanoparticles-Anchored Pramipexole Attenuates the Rotenone-Induced Phenotypes in a *Drosophila* Parkinson's Disease Model

Ramesha Hanumanthappa, Deepa Mugudthi Venugopal, Nethravathi P C, Ahesanulla Shaikh, Siddaiah B.M, Geetha B. Heggannavar, Akshay A. Patil, Hemalatha Nanjaiah, D. Suresh, Mahadevappa Y. Kariduraganavar, Shamprasad Varija Raghu,* and Kuramkote Shivanna Devaraju*

Read Online

ACCESS | Metrics & More | Article Recommendations | SI Supporting Information

ABSTRACT: Parkinson's disease (PD) is a progressive, age-related neurodegenerative disease. The disease is characterized by the loss of dopaminergic neurons in the substantia nigra, pars compacta of the midbrain. Pramipexole (PPX) is a novel drug used for the treatment of PD. It has a high affinity for the dopamine (DA) D2 receptor subfamily and acts as a targeted mitochondrial antioxidant. It is less effective in the treatment of PD due to its short half-life, highly inconvenient dosing schedule, and long-term side effects. In recent years, PPX-loaded nanoformulations have been actively reported to overcome these limitations. In the current study, we focused on increasing the effectiveness of PPX by minimizing the dosing frequency and improving the treatment strategy for PD. Herein, we report the synthesis of biodegradable polyvinylpyrrolidone (PVP)-capped copper oxide nanoparticles (PVP−CuO NPs), followed by PPX anchoring on the surface of the PVP−CuO NPs (PPX−PVP−CuO NC), in a simple and inexpensive method. The newly formulated PPX−PVP−CuO NC complex was analyzed for its chemical and physical properties. The PPX−PVP−CuO NC was tested to protect against rotenone (RT)-induced toxicity in the *Drosophila* PD model. The in vivo studies using the RT-induced *Drosophila* PD model showed significant changes in negative geotaxis behavior and the level of DA and acetylcholinesterase. In addition, oxidative stress markers such as glutathione-*S*-transferase, total glutathione, thiobarbituric acid reactive species, and protein carbonyl content showed significant amelioration. The positive changes of PPX−PVP−CuO NC treatment in behavior, neurotransmitter level, and antioxidant level suggest its potential role in mitigating the PD phenotype. The formulation can be used for treatment or pharmacological intervention against PD.
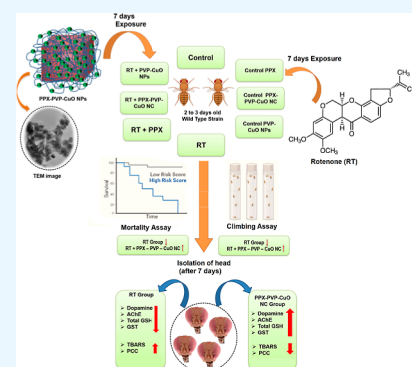
1. INTRODUCTION

Parkinson's disease (PD) is one of the most common neurodegenerative diseases for people at the age of 60−65 years and affects millions of people worldwide.[1] The condition is characterized by decreased level of dopamine (DA) due to the progressive degeneration of the dopaminergic neurons in the substantia nigra pars compacta of the midbrain.[2] It leads to motor symptoms, such as bradykinesia, akinesia, muscle stiffness, and difficulty in walking and coordination, and nonmotor symptoms like autonomic dysfunction, hyposmia, rapid eye moment, sleep behaviors, and cognitive changes.[3,4] The neuropathological hallmark of PD is the accumulation and aggregation of the overexpressed α-synuclein protein in striatal neurons called Lewy bodies, and they are responsible for the degeneration of dopaminergic neurons.[5] Increased oxidative stress is indeed considered to be involved in the death of nigral cells.[6] However, to date, there is no effective treatment that could regenerate dopaminergic neurons. Levodopa is a stable therapeutic PD drug and acts directly as a DA receptor agonist.[7] However, long-term levodopa therapy causes

abnormal involuntary movements, called dyskinesia and dystopia.[8] Levodopa rapidly gets metabolized, and the combination of levodopa along with some adjunct drugs such as carbidopa and entacapone is used to prevent its rapid metabolism in the plasma. However, the longstanding combination treatment of levodopa and carbidopa also causes several side effects.[9,10] For this purpose, ropinirole, bromocriptine, pergolide, cabergoline, and pramipexole (PPX) are used as a first-line treatment with or without levodopa to prevent the symptoms of PD.[11,12]

PPX is a novel drug for the treatment of PD, and it was approved by the Food and Drug Administration (FDA) in 1997. It is a benzothiazole derivative with high affinity as a DA
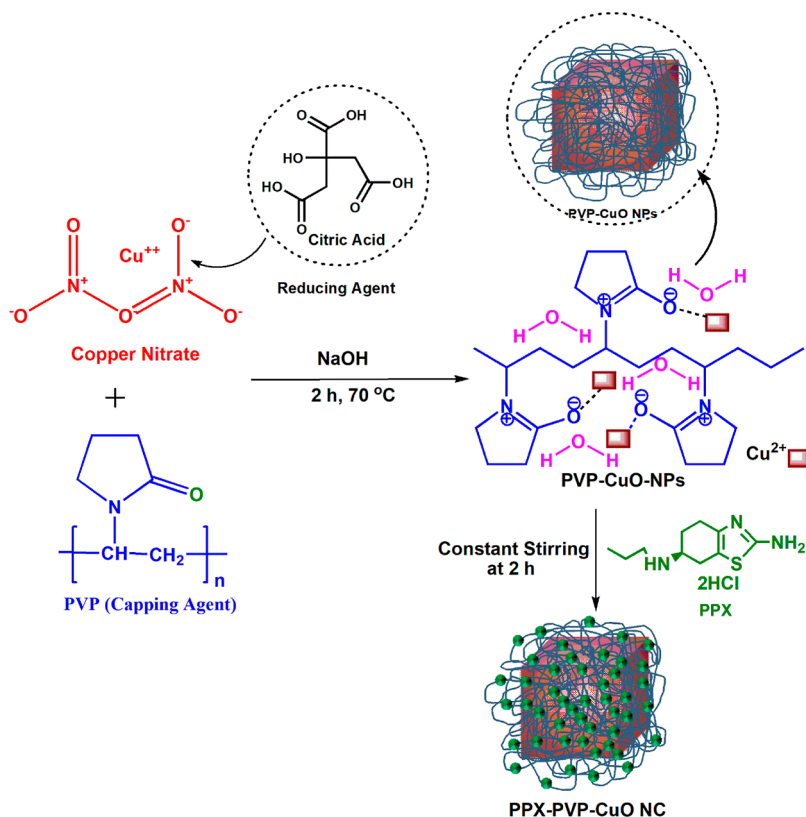
Scheme 1. Schematic Representation of the Synthesis of PVP−CuO NPs and PPX−PVP−CuO[a]

[a]PVP, polyvinylpyrrolidone; PPX, pramipexole dihydrochloride; PVP−CuO NPs, polyvinylpyrrolidone-capped copper oxide nanoparticles; PPX−PVP−CuO NC polyvinylpyrrolidone-capped copper oxide nanoparticles-anchored pramipexole nanocomposite.

D2 receptor subfamily agonist.[13] PPX has been reported to act as a targeted mitochondrial antioxidant, reducing the production of hydrogen peroxide in mitochondria and increasing the activity of aconitase in mitochondria.[14] However, PPX is less effective because of its short half-life and rigorous and highly inconvenient dosing schedule.[15] Lipford and Silber reported that increased doses of PPX showed higher levels of side effects.[16] According to Radio Constantinescu's reported data, the highest dosage of PPX (6 mg/day) leads to neuropsychiatric effects, such as sleep disturbances, akinesia nausea, constipation, postural hypotension, peripheral edema, impulse control disorders, and hallucinosis.[17,18]

The drug nanoparticles (NPs) formulation is one of the powerful nanotechnologies for the future of the pharmaceutical market, nanomedicine, and health systems.[19] Because they can effectively reach the targeted site, control the drug release over a period of time, and improve the plasma half-life of the drug, they can reduce the drug exposure to adverse conditions in the GI tract and minimize the dosage of the loaded drug.[20] They show increased stability against pH, heat, proteases, and destructive structural factors.[21] In recent years, copper oxide NPs (CuO NPs) synthetic methods have been extensively reported as copper is one of the essential elements of the human brain for development, maturation, and function. Also, it is a cofactor of some key metabolic enzymes such as tyrosinase and superoxide dismutase (SOD). CuO NPs show potential therapeutic properties like antitumor, antimicrobial, photocatalysis, biosensing, and so forth.[22] Merrifield et al. reported that PVP capped cerium oxide NPs have high

therapeutic effects against oxidative stress in PD-induced mice.[23] Alaraby et al.[24] reported that in *Drosophila melanogaster*, a low dosage of CuO NPs inhibits repair mechanisms and antioxidative systems against potassium dichromate. Polyvinylpyrrolidone (PVP) is a biodegradable polymer. It acts as a colloidal stabilizer to prevent the aggregation of NPs and serves as the capping agent on the surface of the CuO NPs. PVP-capped CuO NPs were less cytotoxic compared to uncapped CuO NPs.[25] A 0.95 mg/mL concentration of CuO NPs showed 80% larval viability growth in *D. melanogaster*.[26] Baghayeri et al.[27] reported that palladium-PPX-functionalized-multiwalled carbon nanotubes (pd/pp-MWCNTs) were able to detect the low level of DA in human plasma and urine.

D. melanogaster is an excellent model organism in neuro-science research and is used for investigating neurodegenerative disorders such as PD, Alzheimer's disorder (AD), epilepsy, and so forth.[28−30] *D. melanogaster* strongly depicts most allied PD in humans, such as DJ-1, parkin, PINK1 (PTEN-induced putative kinase1), and leucine-rich repeat kinase 2 (LRRK2) repeats.[31] The adult *Drosophila* brain has 130 dopaminergic neurons.[32] Toxins such as rotenone (RT) and 1-methyl-4-phenyl-1,2,3,6-tetrahydropyridine induce PD in *Drosophila* and so have been used for several PD-related investigations.[33] The naturally occurring RT can cross the blood−brain barrier, which generates PD symptoms in *D. melanogaster*,[34] by inhibiting the complex-1 of the mitochondrial electron transport chain[35] and increasing the reactive oxygen species. Deflection of ATP (adenosine triphosphate) synthesis increases oxidative stress[36] and damages the
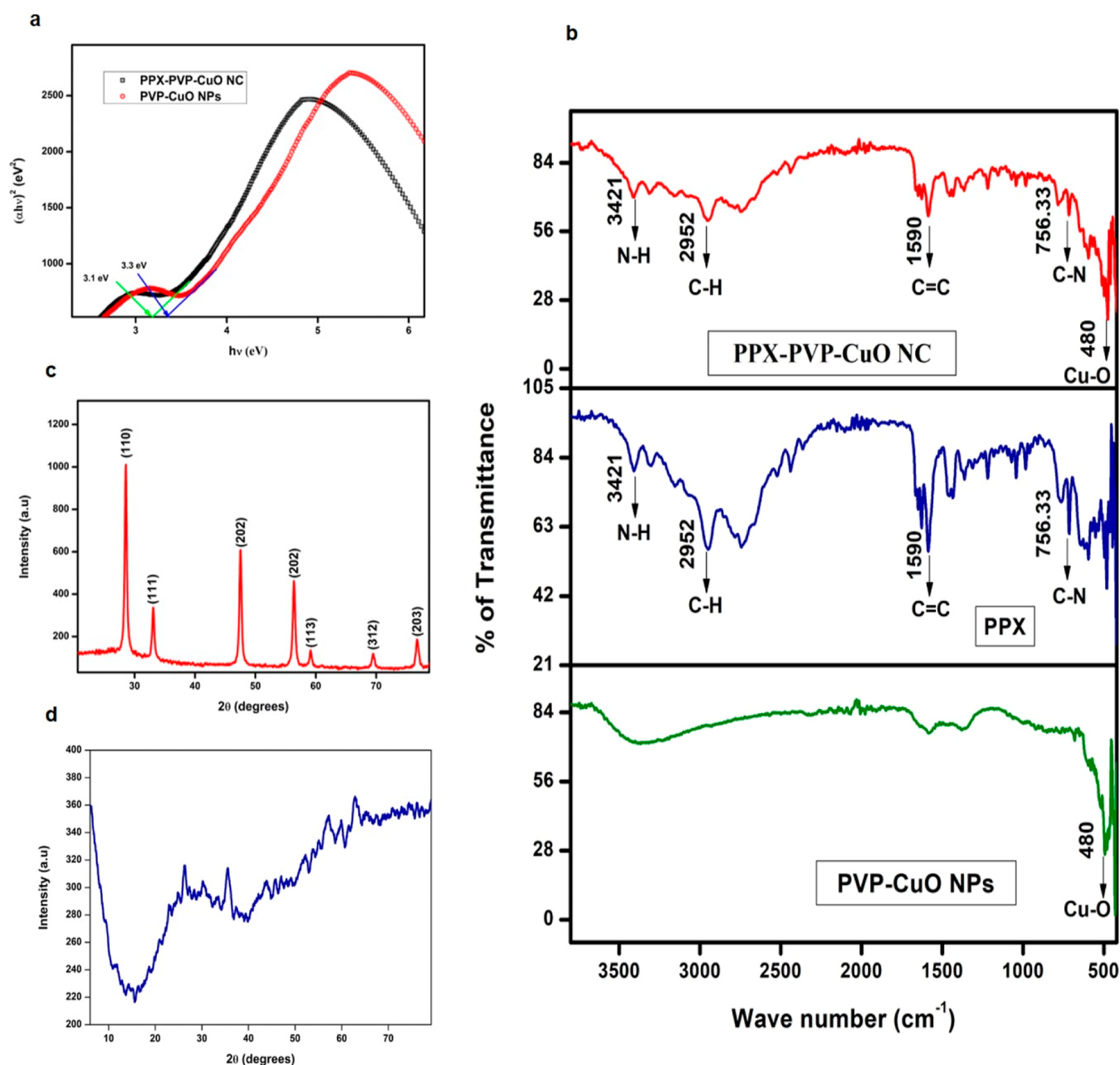
Figure 1. (a) Tauc plots of PVP−CuO NPs and PPX−PVP−CuO NC; (b) FTIR spectra of PVP−CuO NPs, PPX, and PPX−PVP−CuO NC; XRD patterns of (c) PVP−CuO NPs and (d) PPX−PVP−CuO NC.

dopaminergic neurons, leading to cognitive problems and motor symptoms mimicking human PD.[37,38]

In the current study, we have synthesized PVP-capped copper oxide NPs (PVP−CuO NPs), which were further surface-modified with PPX (PPX−PVP−CuO NC). The synthesized nanomaterials were characterized by various techniques, such as UV−visible spectroscopy, Fourier-transform infrared (FTIR) analysis, X-ray diffraction (XRD), field-emission scanning electron microscopy (FE-SEM), energy-dispersive X-ray (EDX) spectrometry, and high-resolution transmission electron microscopy (HR-TEM). PVP is a biodegradable polymer; hence, PVP was used to reduce the toxicity, increase the surface stabilization and dispersibility of the CuO NPs.[39,40] The synthesized PPX−PVP−CuO NC and PVP−CuO NPs were tested against RT-induced oxidative

stress and altered neurotransmitters in the *Drosophila* PD model.

2. RESULTS AND DISCUSSION

2.1. Synthesis and Characterization. In recent decades, nanotechnology-based medicines have played an important role in neurotherapeutics because NPs can carry drugs to a specific site and can increase the bioavailability.[41] The NPs for sustained release of PPX were developed by a precipitation method involving two steps. In the first step, PVP−CuO NPs were synthesized. In the second step, PPX was anchored on the surface of the PVP−CuO NPs (Scheme 1). Here, we used PVP as a capping agent on the surface of CuO NPs because of its biodegradable nature, biocompatibility, as well as temperature and pH stability. It also has excellent solubility and good drug-
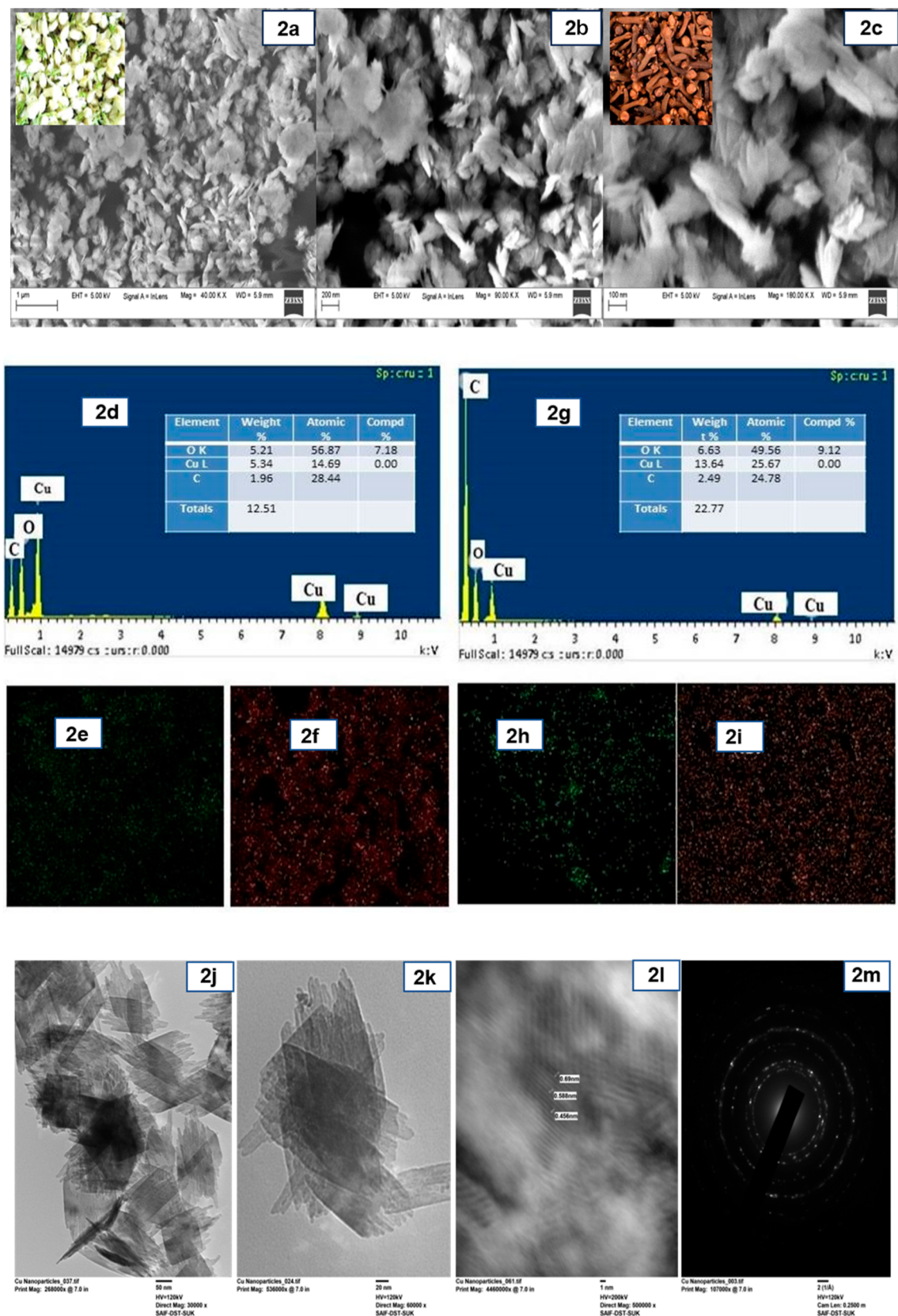
Figure 2. (a,b) FE-SEM images of PVP−CuO NPs (inset: jasmine bud shape), and (c) PPX−PVP−CuO NC (inset: clove bud shape), (d) EDX spectra of PVP−PVP−CuO NPs, (e,f) elemental mapping of PVP−CuO NPs, (g) EDX spectra of PPX−PVP−CuO NC, (h,i) elemental mapping of PPX−PVP−CuO NC; (j−l) HR-TEM images and (m) SAED pattern of PPX−PVP−CuO NC.

binding properties.[40] Thus, it reduces the toxicity and stabilizes the surface to produce good dispersion of the CuO NPs.

Figure 1a illustrates the Tauc plot of PVP−CuO NPs and PPX−PVP−CuO NC. Here, the band gaps of PVP−CuO NPs

as well as of PPX−PVP−CuO NC were determined and were found to be 3.3 and 3.1 eV, respectively. The reduction in the band gap of PPX−PVP−CuO NC is attributed to the considerable interfacial interaction between PVP−CuO NPs and the PPX drug upon encapsulation. The results confirm the successful synthesis of PVP−CuO NPs as well as the encapsulation of the PPX drug.

Figure 1b depicts the FTIR spectra of PVP−CuO NPs, PPX, and PPX−PVP−CuO NC recorded in the 4000 to 400 cm^{-1} range. Characteristic bands at 480, 520, and 600 cm^{-1} were observed and are ascribed to the Cu−O stretching mode of vibration.[42] The bands observed at 3421, 2952, 1590, and 756.33 cm^{-1} correspond to the functional groups N−H twisting, C−H squeezing, C≡C stretching, C−N bending, and C−H bending, respectively, which revealed the composition of typical absorption bands of pure PPX.[43,44] Each of these distinctive patterns due to PVP−CuO NPs as well as PPX were seen in the PPX−PVP−CuO NC spectrum, confirming that there were indeed no chemical associations between the PVP−CuO NPs and PPX.

XRD analysis was performed in the range of 2θ from 5 to 80° for all of the synthesized NPs (PVP−CuO NPs, PPX, and PPX−PVP−CuO NC) to determine their phase purity and crystallinity (Figure 1c,d). Pure PVP−CuO NPs exhibited reflections at 2θ values of 29.7° (110), 36.4° (111), 42.43° (200), 61.35° (220), 73.6° (311), and 77.6° (222) indexed to the cubic phase corresponding to the JCPDS no. 65-3288.[45] No additional peaks were observed due to impurity. This confirms the high purity of the synthesized NPs. The average crystallite size was calculated using the Debye−Scherrer equation, and it was found to be 8.1 nm for PVP−CuO NPs and 12.5 nm for PPX−PVP−CuO NC respectively. On the other hand, when examined with identical 2θ degrees upon encapsulation with PPX of PVP−CuO, the resulting NC failed to exhibit the distinctive crystalline peaks of various baseline elements, demonstrating their total encapsulation by PPX.

$$D = \frac{0.89\lambda}{\beta\cos\theta}$$

where D is the crystallite size, λ is the wavelength of the X-ray source, β is the full width at half-maximum, and θ is Bragg's diffracting angle.

The hydrodynamic size of the developed NP was determined by the dynamic light scattering technique. The resulting data are presented in Figure S1. The data revealed that the hydrodynamic size of the PVP−CuO NPs and PPX−PVP−CuO NC was found to be 62.9 and 112.2 nm, respectively. This clearly shows that PPX was conjugated on the surface of PVP−CuO NPs. leading to an increase in the particle size. To further understand the physical stability of the developed NPs, the zeta potential was measured. The results were found to be −34.5 mV for PVP−CuO NPs and −26.1 mV for PPX−PVP−CuO NPs. This confirms the trend of PPX to PVP−CuO NPs, suggesting that the developed NCs have relatively narrow sizes and better stability.

FE-SEM images of the PVP−CuO NPs and PPX−PVP−CuO NC are shown in Figure 2a−c. FE-SEM images of PVP−CuO NPs resemble the shape of jasmine flower buds with an average particle size of 10−18 nm, as shown in Figure 2a,b. Encapsulation of PPX to the crystal lattice of PVP−CuO NPs leads to the clove-like morphology with slight distortion in the jasmine flower bud-like structure. The average particle size of the PPX−PPV−CuO NC was found to be 15−28 nm (Figure

2c). Minor voids were also observed from the FE-SEM images. The voids were consistently generated and appeared like a globule structure.

The EDX spectra, the composition, and mapping of elements of PVP−CuO NPs and PPX−PVP−CuO NC are depicted in Figure 2d−i. Figure 2d exhibits only peaks due to Cu and O elements, affirming the formation of pure CuO NPs. No other peaks were observed because the synthesized material is highly pure. The insight into the spectra depicts the percentage composition of individual elements shown in Figure 2e,f. In Figure 2g−i, the EDX spectrum of PPX−PVP−CuO NC shows the weight percentage of the elements and further supports the successful encapsulation of PPX drug to PVP−CuO NPs. Elemental mapping analysis results support the EDX spectral results.

TEM, HR-TEM, and selected area electron diffraction (SAED) analyses were conducted to examine the internal morphology of the prepared PPX−PVP−CuO NC, and the results are shown in Figure 2j−l. The TEM image illustrates the unvarying encapsulation of the PPX drug over the surface of PVP−CuO NC which appear like sheets with an average particle size of 12−28 nm. The lattice spacing value was determined from HR-TEM images, which were found to be 0.69 nm (110), 0.588 nm (111), and 0.45 nm (203), which are in good agreement with XRD results. The SAED pattern (Figure 2m) exhibits bright circular fringes that depict the polycrystalline nature of PPX−PVP−CuO NC which are related to (110), (202), and (202) planes of XRD.

2.2. Drug Binding and In Vitro Drug Release. PPX binding on the surface of PVP−CuO NPs and in vitro release of PPX from PPX−PVP−CuO NC were quantified by the internal standard method by using the PPX standard calibration curve at the PPX characteristic peak (λ = 264 nm). The initial ratio of drug and NPs during the synthesis was 1:3 (10 mg of PPX and 30 mg of PVP−CuO NPs) that was arrived with different proportions for effective binding. After completion of the binding, the analysis was carried out for determining the optimum binding of PPX on the surface of PVP−CuO NPs; 6.47 mg of the drug was found to bind to the surface of the PVP−CuO NPs; that is, the drug entrapment efficiency was 64.7%. The release profile of PPX in PPX−PVP−CuO NC was obtained and shown in Figure 3. The release profile indicates that 75.99, 83.85, and 92.87% of PPX were released into the physiological buffer of pH 5.8, 6.8, and 7.4, respectively, within a 24 h period.

2.3. In Vivo *D. melanogaster* Studies. *2.3.1. Survival Assay.* A survival assay was carried out to examine the effect of
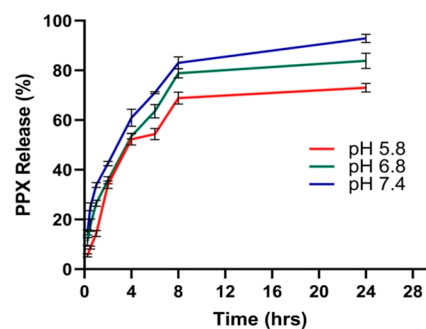

Figure 3. In vitro PPX release from the PPX−PVP−CuO NC at time points of 0.25, 0.50, 1.0, 2.0, 4.0, 6.0, 8.0, and 24.0 h in different physiological buffers of pH 5.8, 6.8, and 7.4.

PPX (10 μg), PPX−PVP−CuO NC (10 μg drug and 46.5 μg NPs), and PVP−CuO NPs (46.5 μg) on the RT-induced toxicity. 2−3 day old flies were exposed to RT in parallel with PPX, PPX−PVP−CuO NC, and PVP−CuO NPs for 7 days and were compared with control groups. As shown in Figure 4,
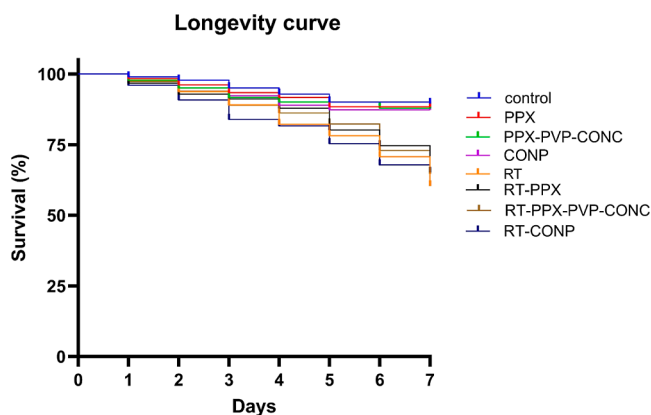

Figure 4. Survival assay for PPX-anchored PVP-capped copper oxide NPs (PPX−PVP−CuO NC), PPX, PVP-capped copper oxide NPs (PVP−CuO NPs), RT, coexposure to RT with PPX−PVP−CuO NC, PPX, and PVP−CuO NPs for 7 days. A significant survival rate ($P > 0.05$) was seen between the RT group with RT plus PPX and RT plus PPX−PVP−CuO NC exposed groups. There was no significant difference between PPX, PPX−PVP−CuO NC, and PVP−CuO NPs exposed group compared to the control group. Mantel−Cox test were used to examine the difference between groups and post hoc pairwise difference. The data is expressed as mean ± SEM of six independent experiments.

Figure 5. Effect of exposure to PPX-anchored PVP-capped copper oxide NPs (PPX−PVP−CuO NC), PPX, PVP-capped copper oxide NPs (PVP−CuO NPs), RT coexposure of RT plus PPX−PVP−CuO NC, PPX, and PVP−CuO NPs for 7 days on the climbing activity of *D. melanogaster*. The number of climbing flies is represented as % of control. Climbing data are expressed as mean ± SEM, for $n = 6$ (each group has 10 numbers), 10 flies escape in 10 s in a 10 cm tube [a indicates a significant difference compared to the control group ($P < 0.05$), b indicates a significant difference compared to the RT group ($p > 0.05$), and c indicates a significant difference compared to RT−PPX and RT−PPX−PVP−CuO NC ($P > 0.05$).

a significant increase in mortality was observed in RT-induced PD flies compared to the control (Mantel−Cox test; $P > 0.001$, ANOVA). But flies exposed to RT plus PPX and PPX−PVP−CuO NC showed reduced mortality compared to the RT-induced PD flies. The control groups which were exposed to PPX, PPX−PVP−CuO NC, and PVP−CuO NPs did not show any significant difference in the survival rate (Mantel−Cox test; $P > 0.05$, ANOVA) compared to RT-unexposed flies group. Interestingly, PPX−PVP−CuO NC and PPX reduced the death rate of flies exposed to RT. A low concentration of PVP−CuO NPs (46.5 μg) also did not induce mortality. Improved or not altered survival rates in PVP−CuO NPs-fed flies suggest less toxicity and promising usage in the *Drosophila* PD model.

2.3.2. Climbing Assay. Locomotor defects resulting from the RT-induced PD model were determined (Figure 5). The RT-induced PD flies showed a significant decrease of 1.78-fold in climbing activity compared to the control flies (Figure 5; F $(7, 56) = 20.37$; $P < 0.05$). The flies exposed to RT plus PPX and the PPX−PVP−CuO NC showed a significant increase of 1.47- and 1.52-fold, respectively, in the climbing activity, compared to RT-induced PD flies (Figure 5; F $(7, 56) = 20.37$; $P < 0.05$). RT plus PVP−CuO NPs did not show any significant increase in climbing activity compared to RT-induced PD flies (Figure 5; F $(7, 56) = 20.37$; $P < 0.05$), and those exposed to RT plus PPX−PVP−CuO NC showed a significant increase of 1.04-fold in climbing activity, compared to RT plus PPX-exposed flies (Figure 5; F $(7, 56) = 20.37$; $P < 0.05$). The control groups PPX, PPX−PVP−CuO NC, and PVP−CuO NPs did not show any significant decrease in the climbing activity compared to the control group (Figure 5; F
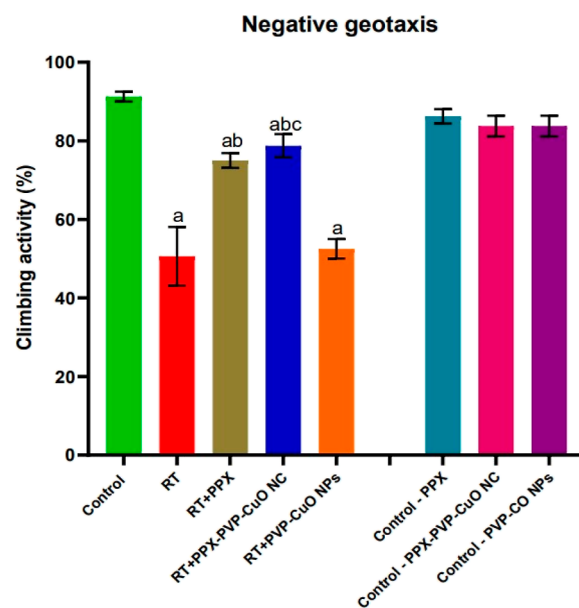
$(7, 56) = 20.37$; $P < 0.05$), as it was reported earlier that PPX effectively improves motor functions and depressive symptoms in PD-induced animal and flies.[46,47] These findings lead to the present observations about the better affinity of PPX−PVP−CuO NC compared to RT-induced PD flies. The RT-induced PD flies lost jumping and flying activity compared to the control group. However, RT plus PPX- and PPX−PVP−CuO NC-exposed flies show improvements in jumping and flying activity compared to RT-induced PD flies at the end of the 7 day experimental period. However, the flies did not recover 100% compared to the control group. Remarkably, the low concentration of PVP−CuO NPs (46.5 μg) did not affect the climbing activity in adult flies.

2.3.3. Determination of DA Levels. The total DA level in *D. melanogaster* exposed to PPX, PPX−PVP−CuO NC, and PVP−CuO NPs and coexposure of RT plus PPX and PPX−PVP−CuO NC was studied for 7 days. The head was separated and used to measure the DA level. The results are listed in Figure 6. The RT-induced PD flies showed a significant decrease of 2.5-fold in the DA level compared to the control flies (Figure 6; F $(7, 16) = 9.633$; $P < 0.05$), which indicates the successful induction of PD. The exposure of RT plus PPX and PPX−PVP−CuO NC showed a significant increase in DA levels by 2.00 and 2.34 folds, respectively, compared to RT-induced PD flies (Figure 6; F $(7, 16) = 9.633$; $P < 0.05$) and RT plus PVP−CuO NPs-exposed flies did not show any significant increase of the DA level compared with RT-induced PD flies (Figure 6; F $(7, 16) = 9.633$; $P < 0.05$). The control groups PPX, PPX−PVP−CuO NC, and PVP−CuO NPs did not show any significant decrease compared to that of the control group in the DA level (Figure 6; F $(7, 16) = $
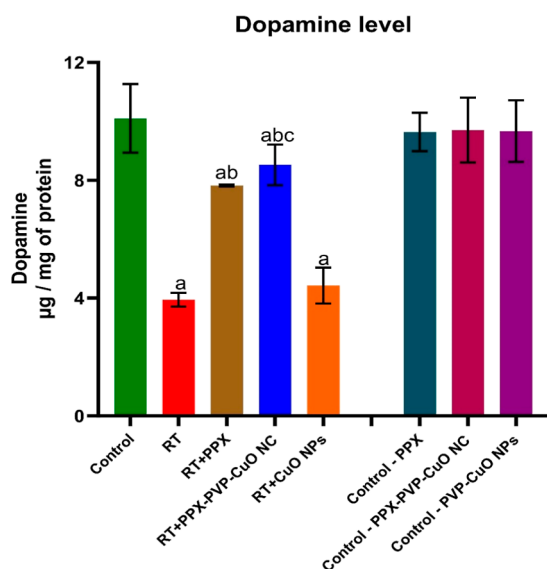
Dopamine level

Acetylcholinesterase

Figure 6. Effect of PPX-loaded PVP-capped copper oxide NPs (PPX−PVP−CuO NC), PPX, PVP-capped copper oxide NPs (PVP−CuO NPs), RT coexposure of RT with PPX−PVP−CuO NC, PPX, and CuO NPs for 7 days, on DA level of *D. melanogaster* head. Data are expressed in mean ± SEM, for $n = 3$ [a indicates a significant difference compared to the control group ($P < 0.05$), b indicates a significant difference compared to the RT group ($p > 0.05$), and c indicates a significant difference compared to RT−PPX and RT−PPX−PVP−CuO NC ($P > 0.05$)].

Figure 7. Effect of PPX-loaded PVP-capped copper oxide NPs (PPX−PVP−CuO NC), PPX, PVP-capped copper oxide NPs (PVP−CuO NPs), RT, and coexposure of RT with PPX−PVP−CuO NC, PPX, and CuO NPs for 7 days, on AChE activity of *D. melanogaster*. Data are expressed as mean ± SEM, for $n = 6$ (each group contains 30 numbers) [a indicates a significant difference compared to the control group ($P < 0.05$), b indicates a significant difference compared to the RT group ($p > 0.05$), and c indicates significant difference compared to RT−PPX and RT−PPX−PVP−CuO NC ($P > 0.05$)].

9.633; $P < 0.05$). PPX is a nonergolinic D3-preferred DA agonist effectively tolerated in treating motor symptoms.[48] It is also reported that treatment with PPX has increased DA level in male rats.[49] In our study, compared to PPX, the PPX−PVP−CuO NC treatment has remarkably restored the DA level in RT-exposed flies. PPX has a very short half-life period,[15] The formulation of PPX−PVP−CuO NC will increase the bioavailability of the PPX and releases the PPX slowly into the system, which helps to maintain constant PPX in the brain for the continued stimulation of DA levels in the brain.

2.3.4. Determination of Acetylcholinesterase Activity. The RT-induced PD flies showed a significant decrease of 3.46-fold in acetylcholinesterase (AChE) activity compared to the control (Figure 7; F (7, 46) = 6.816; $P < 0.05$), which confirms the successful induction of PD. Exposure to RT plus PPX and PPX−PVP−CuO NC showed a significant increase of 2.67- and 2.90-fold, respectively, in the AChE activity, compared to RT-induced PD flies (Figure 7; F (7, 46) = 6.816; $P < 0.05$). RT plus PVP−CuO NPs-exposed flies showed no significant increase in AChE activity, indicating that PVP−CuO NPs alone did not restore the AChE. Exposure to RT plus PPX−PVP−CuO NC showed a substantial increase of 1.11-fold in the AChE activity compared to RT plus PPX-exposed flies (Figure 7; F (7, 46) = 6.816; $P < 0.05$). The control groups PPX, PPX−PVP−CuO NC, and PVP−CuO NPs did not show any significant decrease compared to that of the control group in the AChE activity (Figure 7; F (7, 46) = 6.816; $P < 0.05$). Recent studies have reported that RT alters the AChE activity in *D. melanogaster* and other animal models.[50,51] PPX−PVP−CuO NC exposure showed significant restoration of the AChE activity compared to that of RT-exposed flies and standard PPX drug-exposed flies, as shown in Figure 7.
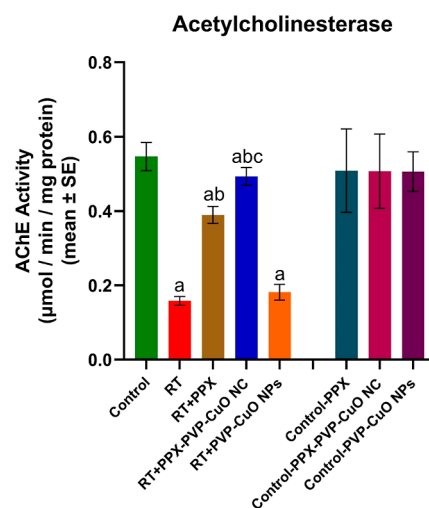
2.3.5. Determination of Total GSH and GST Activity. The effect of exposure to RT (500 μM), PPX (10 μg), PPX−PVP−CuO NC (10 μg drug and 46.5 μg NPs) and PVP−CuO NPs (46.5 μg) and the coexposure of RT and PPX, PPX−PVP−CuO NC, and PVP−CuO NPs for 7 days was studied. The experimental data of total glutathione (GSH) are shown in Figure 8a and glutathione-*S*-transferase (GST) activity is shown in Figure 6b. RT-induced PD flies showed a significant decrease of 2.21-fold in the total GSH activity compared to the control flies (Figure 8a; F (7, 40) = 28.01; $P < 0.05$). However, RT plus PPX and PPX−PVP−CuO NC showed significant increases of 1.40- and 1.58-fold, respectively, in total GSH activity (Figure 8a; F (7, 40) = 28.01; $P < 0.05$) and RT plus PVP−CuO NPs-exposed flies did not show any significant increase of total GSH activity compared with RT-induced PD flies (Figure 8a; F (7, 40) = 28.01; $P < 0.05$). The exposure to RT plus PPX−PVP−CuO NC shows a significant increase of 1.13-fold in total GSH activity compared to the RT plus PPX-exposed flies (Figure 8a; F (7, 40) = 28.01; $P < 0.05$). The control groups PPX, PPX−PVP−CuO NC, and PPX−CuO NPs did not show any significant decrease in total GSH activity compared to the control group (Figure 8a; F (7, 40) = 28.01; $P < 0.05$).

Compared to the control, RT-induced PD flies showed a significant decrease (2.05 folds) in the GST activity (Figure 8b; F (7, 40) = 6.291; $P < 0.05$). The flies exposed to RT plus PPX and PPX−PVP−CuO NC showed a significant increase of 1.36- and 1.78-fold, respectively, in GST activity compared to the RT-induced PD flies (Figure 8b; F (7, 40) = 6.291; $P < 0.05$). The RT plus PVP−CuO NPs-exposed flies did not show any significant increase in GST activity compared with RT-induced PD flies (Figure 8b; F (7, 40) = 6.291; $P < 0.05$). The flies exposed to RT plus PPX−PVP−CuO NC showed a significant increase of 1.30-fold in total GSH activity compared to the RT plus PPX-exposed flies (Figure 8b; F (7, 40) = 6.291; $P < 0.05$). The control groups PPX, PPX−PVP−CuO
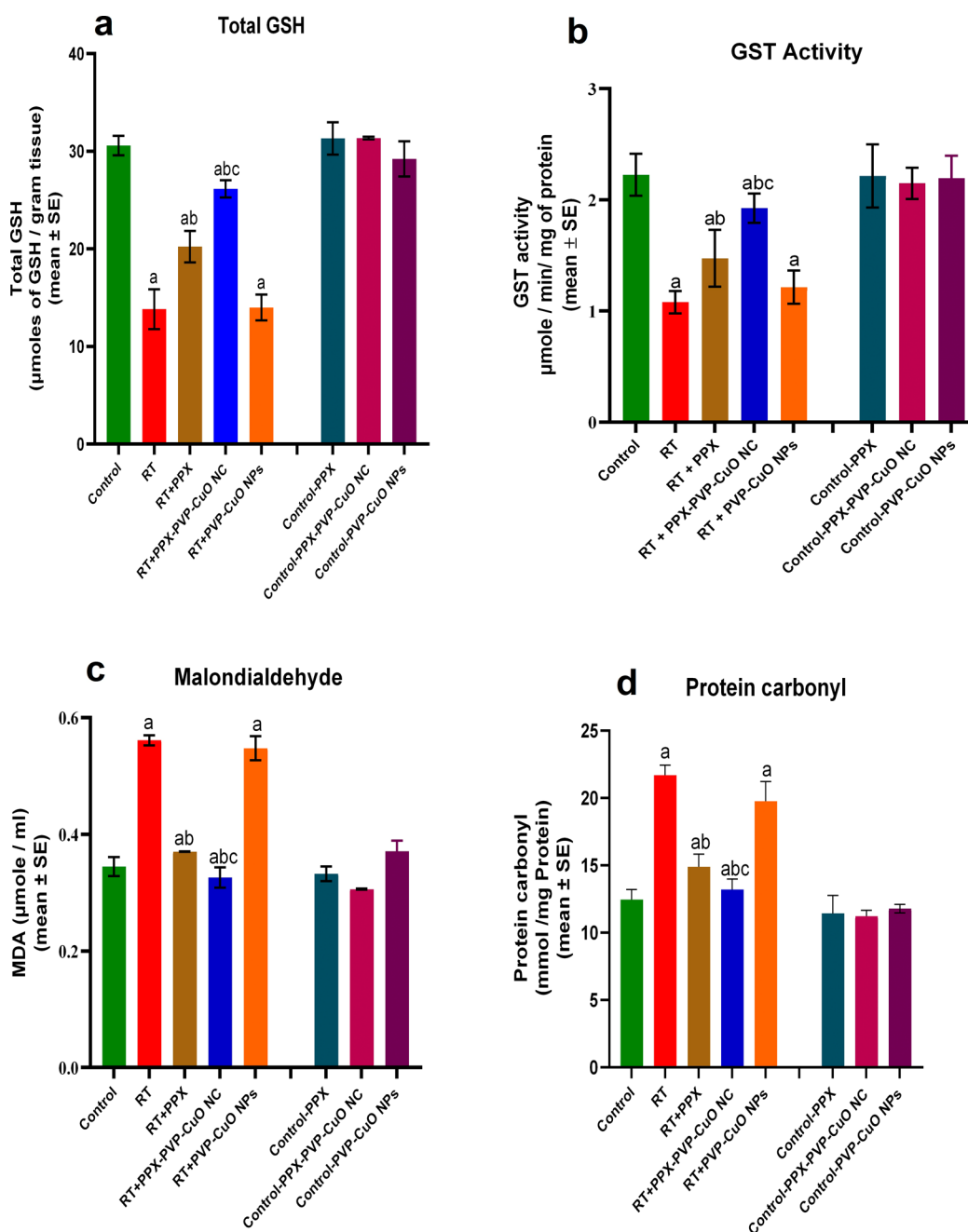
Figure 8. Effect of PPX-loaded PVP-capped copper oxide NPs (PPX−PVP−CuO NC), PPX, PVP-capped copper oxide NPs (PVP−CuO NPs), RT coexposure of RT with PPX−PVP−CuO NC, PPX, and CuO NPs for 7 days, on (a) total GSH, (b) GST activity, (c) malondialdehyde, and (d) protein carbonyl of *D. melanogaster*. Data are expressed as mean ± SEM, for $n = 6$ (each group contains 30 numbers) [a indicates a significant difference compared to the control group ($P < 0.05$), b indicates a significant difference compared to the RT group ($p > 0.05$), and c indicates significant difference compared to RT−PPX and RT−PPX−PVP−CuO NC ($P > 0.05$).

NC, and PPX−CuO NPs did not show any significant decrease in GST activity compared to the control group (Figure 8b; F $(7, 40) = 6.291$; $P < 0.05$).

GSH, a potential antioxidant, plays a vital role in the event of neurodegenerative disorders like Parkinson's, Alzheimer's, and so forth,[52] The GSH levels decreased upon RT exposure in flies and mice.[53,54] In this study, it was observed that RT significantly decreased the total GSH activity, and PPX−PVP−CuO NC remarkably restored the GSH activity in RT-induced PD flies. GST is a phase II family of cysteine-rich multifunctional enzyme domains that helps conjugate GSH with electrophilic molecules to detoxify xenobiotics.[55] The observed

GST inhibition in the RT-exposed flies indicates GST's dysfunctional and detoxification capacity.[56,57] Treatment with PPX−PVP−CuO NC further strengthened the antioxidant capacity in RT-treated flies.

2.3.6. Determination of Malondialdehyde and Protein Carbonyl Content. The effect of exposure to RT (500 μM), PPX (10 μg), PPX−PVP−CuO NC (10 μg drugs and 46.5 μg NPs), and PVP−CuO NPs (46.5 μg) and the coexposure of RT and PPX, PPX−PVP−CuO NC, and PVP−CuO NPs for 7 days was analyzed for total MDA (malondialdehyde) activity and protein carbonyl content (PCC). The MDA and PCC experimental data are presented in Figure 8c,d, respectively.

The MDA activity increased significantly by 1.60-fold in the RT-induced PD flies compared to control flies (Figure 8c; F (7, 40) = 52.45; $P < 0.05$). Flies treated with RT along with PPX and PPX−PVP−CuO NC showed significant decrease of 1.52- and 1.71-fold, respectively, in MDA activity, compared to RT-induced PD files (Figure 8c; F (7, 40) = 52.45; $P < 0.05$), and there is no significant changes in MDA activity compared to RT plus PVP−CuO NPs-treated flies to RT-induced PD flies (Figure 8c; F (7, 40) = 52.45; $P < 0.05$). Exposure to RT plus PPX−PVP−CuO NC showed a significant decrease of 1.13-fold in MDA activity compared to the RT plus PPX-exposed flies (Figure 8c; F (7, 40) = 52.45; $P < 0.05$). The control groups PPX, PPX−PVP−CuO NC, and PVP−CuO NPs did not show any significant changes in MDA activity compared to that of control flies (Figure 8c; F (7, 40) = 52.45; $P < 0.05$).

The RT-induced PD flies showed a significant increase of 1.74-fold in the PCC levels compared to the control group (Figure 8d; F (7, 40) = 18.89; $P < 0.05$). RT plus PPX- and PPX−PVP−CuO NP-treated flies showed a significant decrease of 1.99- and 2.16-fold, respectively, in PCC, compared to RT-induced PD flies (Figure 8d; F (7, 40) = 18.89; $P < 0.05$). PVP−CuO NPs plus RT treatment group did not show any significant changes in PCC activity compared to the RT-induced PD flies (Figure 8d; F (7, 40) = 18.89; $P < 0.05$). The RT plus PPX−PVP−CuO NC-exposed flies showed a significant decrease of 0.92-fold in PCC activity compared to RT plus PPX-exposed flies (Figure 8d; F (7, 40) = 18.89; $P < 0.05$). The control groups PPX, PPX−PVP−CuO NC, and PVP−CuO NPs did not show any significant difference in PCC activity compared to that of the untreated control group (Figure 8d; F (7, 40) = 18.89; $P < 0.05$).

RT increases the oxidative stress that leads to the formation of Lewy bodies,[54] causing damage to dopaminergic neurons.[58] Therefore, the study includes the thiobarbituric acid reactive species (TBARS) and PCC levels in RT-induced PD flies. Previous studies showed that PPX-loaded NPs inhibit the TBARS levels in RT-induced mice.[59] Here, it is observed that the PPX−PVP−CuO NC strongly inhibited the TBARS level in RT-exposed flies. In various mechanisms, protein carbonylation was observed, including the conjugation of an aldehyde with the amine group of amino acids to become a product of conjugated lipids.[60] These include carbonylated proteins that have a long half-life. Hence, the assessment of carbonyl group content indicates the amount of oxidative stress under disease conduction.[61] PPX remarkably inhibits the PCC level in UAS-Hsap/SNCA.F mutant *D. melanogaster*, and our study also resonates with the observations revealed in Siddique et al.[62]

3. CONCLUSIONS

This study reports a new formulation of PVP-capped copper oxide NPs-anchored PPX nanocomposite (PPX−PVP−CuO NC). The compound was tested against the RT-induced *Drosophila* PD model. PPX−PVP−CuO NC treatment was compared with PPX and RT treatments to evaluate its efficiency. The PPX (10 μg), PPX−PVP−CuO NC (10 μg drugs and 46.5 μg NPs), and PVP−CuO NPs (46.5 μg) were treated against the RT-induced PD model for 7 days. The control groups PPX, PPX−PVP−CuO NC, and PVP−CuO NPs did not show any changes in the survival rate, negative geotaxis, neurotransmitter activity, and stress marker activity compared to control flies. Therefore, PPX−PVP−CuO NC was used further to mitigate the RT-induced PD phenotypes in

Drosophila. The coexposure of RT plus PPX and RT plus PPX−PVP−CuO NC increased the climbing ability compared to RT-induced PD flies; the brain homogenate was used for neurotransmitter and oxidative stress marker studies. RT plus PPX and RT plus PPX−PVP−CuO NC showed a remarkable increase in neurotransmitter and oxidative stress markers compared with RT-induced PD flies. However, RT plus PVP−CuO NPs restored neurotransmitters and oxidative stress markers in RT-induced PD flies. In all experiments, PPX−PVP−CuO NC remarkably restored the negative geotaxis, DA level, AChE activity, total GSH, GST activity, MDA, and PCC, compared with RT-induced PD flies. These results are conclusive and innovative, which strongly supports using new nanoformulated treatment strategies against PD.

4. MATERIALS AND METHOD

4.1. Materials. PPX dihydrochloride (98% high-performance liquid chromatography (HPLC) grade powder; CAS no. 104632-25-9), RT (95%; CAS no. 83-79-4), triethylamine (99%; CAS no.121-44-8), DL-10-camphor sulfonic acid ($C_{10}H_{16}O_4S$; CAS no. 35963-20-3), PVP (molecular weight; 10000; CAS no. 9003-39-8), bovine serum albumin (BSA; CAS no. 9048-46.8), potassium phosphate monobasic (KH_2PO_4; CAS no. 7778-77-0), sodium phosphate dibasic (Na_2HPO_4; CAS no. 7558-79-4), perchloric acid (70%; CAS no.7601-90-3), MDA tetrabutyl ammonium salt (96.08%; CAS no.100689-54-3), Bradford reagent (catalog no. B6916), sulfosalicyclic acid (CAS no. 304851-84-1), and copper(II) nitrate ($Cu(NO_3)_2$) (CAS number: 10031-43-3) were purchased from Sigma-Aldrich, USA. 5,5′-Dithiobis(2-nitrobenzoic acid) (DTNB; CAS no. 69-78-3), 1-chloro-2,4-dinitrobenzene (CDNB; CAS no. 74-11-3), GSH reduced (CAS no. 72-18-4), ethylenediaminetetraacetic acid (EDTA; CAS no. 60-00-4), guanidine hydrochloride (CAS no. 50-01-1), acetylthiocholine iodide (CAS no. 1866-15-5), 2,4-dinitrophenylhydrazine (CAS no. 119-26-6), and sodium hydroxide (NaOH; CAS no. 7558-80-7) were purchased from HIMEDIA Laboratories Private Limited in India. Thiobarbituric acid (TBA; CAS no. 504-17-16) was purchased from Spectrochem, Mumbai, India. All chemicals were of reagent grade and used as received. Millipore water was used in the preparation of all of the aqueous solutions.

4.2. Synthesis of PVP−CuO NPs and PPX−PVP−CuO NC. PVP−CuO NPs were prepared by employing the precipitation method.[63,64] Initially, 100 mL of a 10 mM $Cu(NO_3)_2$ solution and 3.4 mM citric acid were placed in a 250 mL beaker. To the above mixture, 34 mg of PVP was added and stirred for an hour. Further, 2 M NaOH solution was added dropwise with constant stirring to the above mixture. The resulting reaction mixture was stirred for 2 h at 70 °C, leading to the formation of a red-colored precipitate. The red precipitate was collected, washed with water, centrifuged and dried at 50 °C. The obtained PVP−CuO NPs were stored in an airtight container until further use. Similarly, 10 mg of PPX dihydrochloride was dissolved in 20 mL of Milli-Q Water, added to PVP−CuO NPs solution (30 mg) drop-by-drop, and stirred for 2 h at room temperature. Finally, the resulting product was washed with distilled water and lyophilized to get PPX-anchored PVP-capped copper oxide nanocomposite (PPX−PVP−CuO NC), which was stored at 4 °C.[65,66] The schematic representation of the synthesis of NPs is shown in Scheme 1.

4.3. Drug Binding Studies. Drug binding or loading on the surface of PVP–CuO NPs was determined according to Tzankov et al.,[14] and Pahuja et al.,[67] with some modification. Briefly, nonbinding PPX dihydrochloride was found in the supernatant during the coating or anchoring procedure, and the absorbance was measured at 264 nm using a UV–visible spectrophotometer (Shimadzu UV-1800). The concentration of PPX was calculated by using the PPX standard curve (R^2 = 0.984; Figure S2). The loading and entrapment efficiencies were calculated using the following formulas

$$DL\ (\%) = \frac{\text{total amount of PPX} - \text{PPX in supernatant}}{\text{Total weight of NPs}}$$
$$\times 100$$

$$EE\ (\%) = \frac{\text{total amount of PPX in formulation}}{\text{total amount of PPX}} \times 100$$

4.4. Characterization. A UV–visible spectrophotometer (Thermo Scientific Spectrophotometer, Research Lab, Department of Biochemistry, Tumkur University, Tumakuru, India) was used to analyze the optical properties of the prepared PPX, PVP–CuO NPs, and PPX–PVP–CuO NC. The phase purity and crystallinity of the synthesized nanomaterials were analyzed through XRD patterns by using a Cu-rotating anode X-ray generator, an Oxford Cryostream 700 series (100 K), and a photon detector (Sophisticated Analytical Instrument Facility, Karnatak University, Dharwad, India) External and internal morphologies of the nanomaterials were examined through FE-SEM (CARL ZEISS FESEM 03-81; University science instrumentation facility, Mangalore University, Mangalore, India). Elemental composition and purity of the synthesized nanomaterials were acquired by using an Oxford instrument energy-dispersive spectrophotometer, UK Germany (University science instrumentation facility, Mangalore University, Mangalore, India) and a high-resolution transmission electron microscope (JEOL ASIA PTE LTD, JEM 2100 PLUS; Sophisticated Analytical Instrument Facility, Shivaji University, Maharashtra, India). FTIR studies were carried out using a Nicolet impact-410 FTIR spectrometer, USA (University science instrumentation facility phase-II, Karnatak University, Dharwad, India). The hydrodynamic size and zeta potential of the developed NPs were determined by using a HORIBA SZ-100 for Windows [Z Type] ver 2.20 (University science instrumentation facility phase-II, Karnatak University, Dharwad, India).

4.5. In Vitro Drug Release Assay. The in vitro PPX release studies were carried out according to Tort et al.,[68] Bahari Javan et al.,[69] and Papadimitriou et al.[70] by using dialysis membrane (HIMEDIA; molecular cutoff, 10 kDa). This method dispersed 2.0 mg of PPX–PVP–CuO NC in 1 mL of phosphate buffer (pH: 5.8 and 6.8) and phosphate buffer saline (pH 7.4). The dispersed PPX–PVP–CuO NC was inserted into respective dialysis membranes. The dialysis membranes were immersed in 25 mL of the respective buffer media (phosphate buffer, pH 5.8 and 6.8 and phosphate buffered saline, pH 7.4) and incubated at room temperature using a magnetic stirrer (500 rpm/min). At predetermined time points (0.25, 0.50, 1.0, 2.0, 4.0, 6.0, 8.0, and 24.0 h), 1.0 mL of buffer was collected, and the fresh buffer was replaced with respective pH buffers. The amount of released PPX from the PPX–PVP–CuO NC was measured at 264 nm.

4.6. *D. melanogaster* Stock. Wild-type *D. melanogaster* (Canton-S) was obtained from the University of Mysore

Drosophila Stock Centre, Mysore, Karnataka. The flies were reared in a 2.5 × 6.0 cm tube containing 5 mL of wheat cream media (10% w/v jaggery; 10% w/v rava; 1% w/v agar; and 0.75% w/v propionic acid) at a constant temperature of 25 ± 1 °C and 75% of humidity, under the 12 h dark and 12 h light cycle. All experiments were performed with the same strain.

4.7. Experimental Design. One to three day old flies were divided into eight groups (30 flies in each group). (1) control; (2) PPX control; (3) PPX–PVP–CuO NC control; (4) PVP–CuO NPs control; (5) RT control; (6) RT plus PPX; (7) RT plus PPX–PVP–CuO NP; and (8) RT plus PVP–CuO NPs; all were exposed to drugs via diet until 7 days of the experiment. The control group was provided only a standard diet and exposed to PPX (10 mg), PPX–PVP–CuO NC (10 μg drug and 46.5 μg NPs), and PVP–CuO NPs (46.5 μg), respectively, with 15% brewer's yeast and were exposed to 500 μM RT along with 15% brewer's yeast. For the treatment group, flies were exposed to PPX (10 μg), PPX–PVP–CuO NC (10 μg drug and 46.5 μg NPs), and PVP–CuO NPs (46.5 μg) and mixed with 500 μM of RT and 15% brewer's yeast. All the experiments were repeated six times (*n* = 6). After 7 days of exposure, the climbing assay was conducted. The separated heads were homogenized and used for all of the biochemical assays.

4.8. Survival Assay. The survival assay[71,72] was performed by daily counting of living flies until the end of the experiments (7 days); flies were maintained at 25 ± 1 °C (12 h light/dark cycle); 180 flies per group were included in the survival data, and the total number of flies represents the sum of six (*n* = 6) independent experiments (30 flies per each treatment group).

4.9. Negative Geotaxis Assay. The locomotor ability of the control and treated groups was tested using a negative geotaxis assay described previously by Singh et al.[73] and Feany and Bender.[74] Both control and treatment flies were anesthetized with an ice pack, and 10 flies were placed in a vertical glass cylinder (15 cm in length and 2.0 cm in diameter). The flies that reached the 10 cm length of the column and the flies that remained at the bottom were counted separately for 10 s. The data represent the mean of the number of flies at the top as a percentage of the total number of flies. This value represents the sum of six (*n* = 6) independent experiments.

4.10. Homogenate Preparation for Biochemical Assays. The flies were selected from six sets of experiments and anesthetized with ice. Carefully, the head was separated from the body, homogenized in 0.1 M phosphate buffer (pH 7.4, 1 head: 5 μL buffer), and centrifuged at 7000 RCF for 10 min (REMI cooling centrifuge C-24 BL). Supernatants were collected and used for the determination of the following biochemical parameters: protein estimation, AChE, total GSH, PCC, TBARS, and DA level.

4.11. Homogenate Preparation for HPLC with Electrochemical Detection. For high-performance liquid chromatography (HPLC), 40 heads were homogenized in 200 μL of 0.2 N perchloric acid, followed by centrifugation (5000 rpm) for 10 min at −4 °C (REMI cooling centrifuge C-24 BL). The homogenate was further filtered through a 0.2 μm syringe (AXIVA syringe filter nylon-13 mm/0.2 μm) and stored at −80 °C until use.

4.12. Total Protein Determination. The total protein concentration of flies' head homogenates was estimated according to the Bradford method[75] using BSA as the standard.

4.13. HPLC with Electrochemical Detection for Measuring DA Levels. The brain DA levels were quantified according to the method developed by Carvajal-Oliveros et al.,[76] Maheswari et al.,[77] and Das et al.,[78] with slight modification. Briefly, 20 μL of brain homogenate was injected into a HPLC system with a C-18 column (Spherisorb, RP C18, 5 μm particle size, 4 mm × 250 mm at 30 °C) and equipped with an electrochemical detector (model 1645, Waters, USA). The mobile phase consists of 17.6% of methanol, 82.4% of water, 0.0876 mM of EDTA, 1.5 mM TEA, 9 mM of DL-$C_{10}H_{16}O_4S$, 20 mM Na_2HPO_4, and 15 mM citric acid; it was pumped at a flow rate of 0.7 mL/min. The standard was injected separately, and the retention time was found to be 4.21 min for DA. The DA concentration in the samples was analyzed by comparing it with the peak area of standard and expressing it in μg/mg of protein.

4.14. Determination of AChE Activity. AChE activity was determined according to the method of Bianchini et al.[79] The reaction mixture contained 135 μL of distilled water, 20 μL of 100 mM potassium phosphate buffer (pH 7.4), 20 μL of 10 Mm DTNB, 5 μL of homogenate, and 20 μL of 8 mM acetylthiocholine as the inhibitor. The reaction mixture was observed at 412 nm using a Thermo Scientific GENESYS 50, version 2.6 for 5 min at 15 s intervals. The AChE activity was expressed as μmol/min/mg protein.

4.15. Estimation of GST. GST was estimated according to Habig and Jakoby[80] using the substrate CDNB. The reaction mixture contained 250 μL of GSH solution (0.1 M GSH). 10.5 mL of distilled water, 2.5 mM EDTA, 20 mL of 0.25 M potassium phosphate buffer (pH-7.4), 20 μL of sample, and 10 μL of 25 mM CDNB. The absorbance of the reaction mixture was measured for 5 min at every 10 s interval using Thermo Scientific GENESYS 50, version 2.6; the data were expressed as μmol/min/mg protein.

4.16. Estimation of GSH Content. GSH content was estimated according to the method described by Jollow et al.,[81] using Ellman's reagent. 60 μL of homogenate was precipitated with 60 μL of sulfosalicylic acid (4%, 1:1 ratio), and the sample was incubated at 4 °C for 1 h. The resultant precipitate was centrifuged at 2600g for 10 min at 4 °C. Finally, the reaction mixture containing 0.1 M phosphate buffer (pH 7.4, 550 μL), 100 μL of supernatant, and DNTB (100 μL), observed at 412 nm, and data were expressed as μ mol of GSH per g tissue.

4.17. Determination of MDA Level. MDA was determined, as described by Spirlandeli et al.,[82] for measuring the formation of TBARS. The reaction mixture containing 100 μL of homogenate, and 1 mL of solution A [solution A: TCA 15%), TBA (0.38%), and 0.25 M hydrochloric acid] was heated at 100 °C for 30 min, which was further allowed to interact in ice cold water for 2 min. Later, the solution was centrifuged at 7000 rpm for 5 min, the related absorbance was read at 370 nm, and data were expressed in μmol of MDA produced per mL.

4.18. Estimation of PCC. Estimation of PCC was carried out using the method described by Siddique et al.[83] The reaction mixture containing approximately 1 mg/mL of brain homogenate was mixed in an Eppendorf centrifuge tube containing 2 4-dinitrophenyl hydrazine (250 μL). The tubes were vortexed in a dark place for 20 min. Later, 125 μL of TCA (50%) was added to this reaction mixture and incubated at −20 °C for 15 min. Further, the reaction mixture was centrifuged at 4 °C for 10 min at 9000 rpm. The obtained pellet was washed with equal volumes of ice-cold ethanol and ethyl acetate. Lastly, the pellets were resuspended in 1000 μL of guanidine hydrochloride (6 M), and the absorbance was measured at 370 nm. The PCC content was quantified using a molar absorption coefficient of 22,000 M^{-1} cm^{-1}.

4.19. Statistical Analysis. The Graph Pad Prism 8.3.1 software was used for statistical analysis and plotting graphs; for ANOVA (one-way) followed by Tukey's post hoc test, values of $P > 0.05$ and for the survival assay Mental−Cox test values of $P > 0.05$ were considered statistically significant. All results were expressed as mean ± SEM of six independent experiments.

ASSOCIATED CONTENT

Supporting Information

The Supporting Information is available free of charge at https://pubs.acs.org/doi/10.1021/acsomega.3c04312.

Zeta potential and zeta size results of PVP−CuO NPs and PPX−PVP−CuO NC, PPX standard calibration curve, and DA standard curve (PDF)

AUTHOR INFORMATION

Corresponding Authors

Shampsrasad Varija Raghu − Neurogenetics Lab, Department of Applied Zoology, Mangalore University, Mangalagangothri, Karnataka 574199, India; Division of Neuroscience, Yenepoya Research Centre (YRC), Yenepoya (Deemed to be University), Mangalore, Karnataka 575018, India; Email: shamprasadvr@yenepoya.edu.in

Kuramkote Shivanna Devaraju − Neuro-chemistry Lab, Department of Biochemistry, Karnatak University, Dharwad, Karnataka 580003, India; orcid.org/0000-0002-6199-354X; Email: ksdevaraju@kud.ac.in

Authors

Ramesha Hanumanthappa − Neuro-chemistry Lab, Department of Biochemistry, Karnatak University, Dharwad, Karnataka 580003, India

Deepa Mugudthi Venugopal − Neurogenetics Lab, Department of Applied Zoology, Mangalore University, Mangalagangothri, Karnataka 574199, India

Nethravathi P C − Department of Studies and Research in Organic Chemistry, and Department of Chemistry, University Collage of Science, Tumkur University, Tumkur, Karnataka 572103, India; orcid.org/0000-0003-4703-6708

Ahesanulla Shaikh − Neuro-chemistry Lab, Department of Biochemistry, Karnatak University, Dharwad, Karnataka 580003, India

Siddaiah B.M − Neuro-chemistry Lab, Department of Biochemistry, Karnatak University, Dharwad, Karnataka 580003, India

Geetha B. Heggannavar − Department of Chemistry, Karnatak University, Dharwad, Karnataka 580003, India

Akshay A. Patil − Department of Botany, Karnataka Science College, Dharwad, Karnataka 580001, India

Hemalatha Nanjaiah − Neuro-chemistry Lab, Department of Biochemistry, Karnatak University, Dharwad, Karnataka 580003, India; Department of Microbiology and Immunology, University of Maryland School of Medicine, Baltimore, Maryland 21201, United States

D. Suresh − Department of Studies and Research in Organic Chemistry, and Department of Chemistry, University Collage

of Science, Tumkur University, Tumkur, Karnataka 572103, India

Mahadevappa Y. Kariduraganavar − Department of Chemistry, Karnatak University, Dharwad, Karnataka 580003, India; ⊙ orcid.org/0000-0002-2159-0543

Complete contact information is available at:
https://pubs.acs.org/10.1021/acsomega.3c04312

Author Contributions

Conceptualization: Ramesha Hanumanthappa, Kuramkote Shivanna Devaraju, and Shamprasad Varija Raghu. Methodology: Ramesha Hanumanthappa, Deepa Mugudthi Venugopal, Ahesanulla Shaikh, and Nethravathi P C. Visualization: Kuramkote Shivanna Devaraju, Shamprasad Varija Raghu, Mahadevappa Y Kariduraganavar, and D Suresh. Writing: Ramesha Hanumanthappa, Geetha B Heggannavar, and Akshay A Patil. Data Interpretation and Editing: Ramesha Hanumanthappa, Hemalatha Nanjaiah, Geetha B Heggannavar, Siddaiah B. M, and Nethravathi P C. Validation: Kuramkote Shivanna Devaraju, Shamprasad Varija Raghu, Mahadevappa Y Kariduraganavar, and D Suresh. Graphical abstract: Ramesha Hanumanthappa and Geetha B Heggannavar. Resources: Ramesha Hanumanthappa, Kuramkote Shivanna Devaraju, Ahesanulla Shaikh, and Siddaiah B.M.

Notes

The authors declare no competing financial interest.

■ ACKNOWLEDGMENTS

■ ABBREVIATIONS

NPs, nanoparticles; PD, Parkinson's disease; AD, Alzheimer's disease; PINK1, PTEN-induced putative kinase 1; LRRK2, leucine-rich repeat kinase 2; PPX, pramipexole; RT, rotenone; PVP, polyvinylpyrrolidone; Cu_2O NPs, copper oxide nanoparticles; PVP−CuO NPs, polyvinylpyrrolidone-capped copper oxide nanoparticles; PPX−PVP−CuO NC, polyvinylpyrrolidone-capped copper oxide nanoparticles-anchored pramipexole; DA, dopamine; AChE, acetyl cholinesterase; GSH, glutathione; TBARS, thiobarbituric acid reactive species; PCC, protein carbonyl content; SOD, superoxide dismutase; ATP, adenosine triphosphate; CDNB, 1-chloro-2,4-dinitrobenzene; DTNB, 5,5′-dithiobis(2-nitrobenzoic acid); GSH, glutathione reduced; EDTA, ethylenediaminetetraacetic acid; BSA, bovine serum albumin; DPA, 2,4-dinitrophenylhydrazine; TBA, thiobarbituric acid; K_2HPO_4, potassium dihydrogen phosphate; KH_2PO_4, potassium phosphate monobasic; Na_2HPO_4, sodium phosphate dibasic; NaH_2PO_4, sodium phosphate monobasic; NaOH, sodium hydroxide; TEA, triethylamine; $Cu(NO_3)_2$, copper(II) nitrate

■ REFERENCES

(1) Tang, X.; Xing, S.; Ma, M.; Xu, Z.; Guan, Q.; Chen, Y.; Feng, F.; Liu, W.; Chen, T.; Chen, Y.; Sun, H. The Development and Design Strategy of Leucine-Rich Repeat Kinase 2 Inhibitors: Promising Therapeutic Agents for Parkinson's Disease. J. Med. Chem. 2023, 66 (4), 2282−2307.

(2) Surmeier, D. J. Determinants of dopaminergic neuron loss in Parkinson's disease. FEBS J. 2018, 285 (19), 3657−3668.

(3) Goldenberg, M. M. Medical management of Parkinson's disease. P T 2008, 33 (10), 590−606.

(4) Dong, A. Q.; Yang, Y. P.; Jiang, S. M.; Yao, X. Y.; Qi, D.; Mao, C. J.; Cheng, X. Y.; Wang, F.; Hu, L. F.; Liu, C. F. Pramipexole inhibits astrocytic NLRP3 inflammasome activation via Drd3-dependent autophagy in a mouse model of Parkinson's disease. Acta Pharmacol. Sin. 2023, 44 (1), 32−43.

(5) Gomez-Benito, M.; Granado, N.; Garcia-Sanz, P.; Michel, A.; Dumoulin, M.; Moratalla, R. Modeling Parkinson's Disease With the Alpha-Synuclein Protein. Front. Pharmacol 2020, 11, 356.

(6) Ferrari-Toninelli, G.; Maccarinelli, G.; Uberti, D.; Buerger, E.; Memo, M. Mitochondria-targeted antioxidant effects of S(−) and R(+) pramipexole. BMC Pharmacol. 2010, 10, 2.

(7) Mercuri, N. B.; Bernardi, G. The 'magic' of L-dopa: why is it the gold standard Parkinson's disease therapy? Trends Pharmacol. Sci. 2005, 26 (7), 341−344.

(8) Nakamura, Y. Problems of long-term levodopa therapy in Parkinson's disease. Nihon Rinsho 1997, 55 (1), 65−71.

(9) Müller, T. Levodopa/carbidopa and entacapone in the treatment of Parkinson&rsquo;s disease: efficacy, safety and patient preference. Patient Prefer. Adherence 2009, 3, 51−59.

(10) In Clinical Review Report: Levodopa/Carbidopa (Duodopa): (Abbvie Corporation): Indication: For the treatment of patients with advanced levodopa-responsive Parkinson's disease who do not have satisfactory control of severe, debilitating motor fluctuations and hyper-/dyskinesia despite optimized treatment with available combinations of Parkinson's medicinal products, and, for whom the benefits of this treatment may outweigh the risks associated with the insertion and long-term use of the percutaneous endoscopic gastrostomy-jejunostomy (PEG-J) tube required for administration, Ottawa (ON), 2018.

(11) Shill, H. A.; Stacy, M. Update on ropinirole in the treatment of Parkinson's disease. Neuropsychiatr. Dis. Treat. 2008, 5, 33−36.

(12) Stocchi, F.; Berardelli, A.; Vacca, L.; Thomas, A.; De Pandis, M. F.; Modugno, N.; Valente, M.; Ruggieri, S. Combination of two different dopamine agonists in the management of Parkinson's disease. Neurol. Sci. 2002, 23, S115−S116.

(13) Živec, M.; Anžič, B.; Gobec, S. A Novel Scalable Synthesis of Pramipexole. Org. Process Res. Dev. 2010, 14 (5), 1125−1129.

(14) Tzankov, B.; Voycheva, C.; Yordanov, Y.; Aluani, D.; Spassova, I.; Kovacheva, D.; Lambov, N.; Tzankova, V. Development and in vitro safety evaluation of pramipexole-loaded hollow mesoporous silica (HMS) particles. Biotechnol. Biotechnol. Equip. 2019, 33 (1), 1204−1215.

(15) Li, S.; Liu, J.; Li, G.; Zhang, X.; Xu, F.; Fu, Z.; Teng, L.; Li, Y.; Sun, F. Near-infrared light-responsive, pramipexole-loaded biodegradable PLGA microspheres for therapeutic use in Parkinson's disease. Eur. J. Pharm. Biopharm. 2019, 141, 1−11.

(16) Lipford, M. C.; Silber, M. H. Long-term use of pramipexole in the management of restless legs syndrome. Sleep Med. 2012, 13 (10), 1280−1285.

(17) Constantinescu, R. Update on the use of pramipexole in the treatment of Parkinson&rsquo;s disease. Neuropsychiatr. Dis. Treat. 2008, 4 (2), 337−352.

(18) Holtz, N. A.; Tedford, S. E.; Persons, A. L.; Grasso, S. A.; Napier, T. C. Pharmacologically distinct pramipexole-mediated akinesia vs. risk-taking in a rat model of Parkinson's disease. Prog. Neuro-Psychopharmacol. Biol. Psychiatry 2016, 70, 77−84.

(19) Kumar, R.; Dalvi, S. V.; Siril, P. F. Nanoparticle-Based Drugs and Formulations: Current Status and Emerging Applications. ACS Appl. Nano Mater. 2020, 3 (6), 4944−4961.

(20) Wen, H.; Jung, H.; Li, X. Drug Delivery Approaches in Addressing Clinical Pharmacology-Related Issues: Opportunities and Challenges. *AAPS J.* **2015**, *17* (6), 1327−1340.

(21) Asefy, Z.; Hoseinnejhad, S.; Ceferov, Z. Nanoparticles approaches in neurodegenerative diseases diagnosis and treatment. *Neurol. Sci.* **2021**, *42* (7), 2653−2660.

(22) Verma, N.; Kumar, N. Synthesis and Biomedical Applications of Copper Oxide Nanoparticles: An Expanding Horizon. *ACS Biomater. Sci. Eng.* **2019**, *5* (3), 1170−1188.

(23) Merrifield, R. C.; Wang, Z. W.; Palmer, R. E.; Lead, J. R. Synthesis and Characterization of Polyvinylpyrrolidone Coated Cerium Oxide Nanoparticles. *Environ. Sci. Technol.* **2013**, *47* (21), 12426−12433.

(24) Alaraby, M.; Hernandez, A.; Marcos, R. Copper oxide nanoparticles and copper sulphate act as antigenotoxic agents in drosophila melanogaster. *Environ. Mol. Mutagen.* **2017**, *58* (1), 46−55.

(25) Koczkur, K. M.; Mourdikoudis, S.; Polavarapu, L.; Skrabalak, S. E. Polyvinylpyrrolidone (PVP) in nanoparticle synthesis. *Dalton Trans.* **2015**, *44* (41), 17883−17905.

(26) Carmona, E. R.; Inostroza-Blancheteau, C.; Obando, V.; Rubio, L.; Marcos, R. Genotoxicity of copper oxide nanoparticles in Drosophila melanogaster. *Mutat. Res., Genet. Toxicol. Environ. Mutagen.* **2015**, *791*, 1−11.

(27) Baghayeri, M.; Nodehi, M.; Veisi, H.; Tehrani, M. B.; Maleki, B.; Mehmandost, M. The role of pramipexole functionalized MWCNTs to the fabrication of Pd nanoparticles modified GCE for electrochemical detection of dopamine. *Daru* **2019**, *27* (2), 593−603.

(28) Anupama, K. P.; Antony, A.; Shilpa, O.; Raghu, S. V.; Gurushankara, H. P. Jatamansinol from Nardostachys jatamansi Ameliorates Tau-Induced Neurotoxicity in Drosophila Alzheimer's Disease Model. *Mol. Neurobiol.* **2022**, *59* (10), 6091−6106.

(29) Ayajuddin, M.; Phom, L.; Koza, Z.; Modi, P.; Das, A.; Chaurasia, R.; Thepa, A.; Jamir, N.; Neikha, K.; Yenisetti, S. C. Adult health and transition stage-specific rotenone-mediated Drosophila model of Parkinson's disease: Impact on late-onset neurodegenerative disease models. *Front. Mol. Neurosci.* **2022**, *15*, 896183.

(30) Mituzaite, J.; Petersen, R.; Claridge-Chang, A.; Baines, R. A. Characterization of seizure induction methods in Drosophila. *Eneuro* **2021**, *8* (4), No. ENEURO.0079-21.2021.

(31) Xiong, Y.; Yu, J. Modeling Parkinson's Disease in Drosophila: What Have We Learned for Dominant Traits? *Front. Neurol.* **2018**, *9*, 228.

(32) Karam, C. S.; Jones, S. K.; Javitch, J. A. Come Fly with Me: An overview of dopamine receptors in Drosophila melanogaster. *Basic Clin. Pharmacol. Toxicol.* **2020**, *126* (S6), 56−65.

(33) Munoz-Soriano, V.; Paricio, N. Drosophila Models of Parkinson's Disease: Discovering Relevant Pathways and Novel Therapeutic Strategies. *J. Parkinson's Dis.* **2011**, *2011*, 1−14.

(34) Johnson, M. E.; Bobrovskaya, L. An update on the rotenone models of Parkinson's disease: Their ability to reproduce the features of clinical disease and model gene-environment interactions. *Neurotoxicology* **2015**, *46*, 101−116.

(35) Wang, T.; Li, C.; Han, B.; Wang, Z.; Meng, X.; Zhang, L.; He, J.; Fu, F. Neuroprotective effects of Danshensu on rotenone-induced Parkinson's disease models in vitro and in vivo. *BMC Complementary Med. Ther.* **2020**, *20* (1), 20.

(36) Siima, A. A.; Stephano, F.; Munissi, J. J. E.; Nyandoro, S. S. Ameliorative effects of flavonoids and polyketides on the rotenone induced Drosophila model of Parkinson's disease. *Neurotoxicology* **2020**, *81*, 209−215.

(37) Chia, S. J.; Tan, E. K.; Chao, Y. X. Historical Perspective: Models of Parkinson's Disease. *Int. J. Mol. Sci.* **2020**, *21* (7), 2464.

(38) Hamadjida, A.; Frouni, I.; Kwan, C.; Huot, P. Classic animal models of Parkinson's disease: a historical perspective. *Behav. Pharmacol.* **2019**, *30* (4), 291−310.

(39) Kurakula, M.; Rao, G. K. Pharmaceutical assessment of polyvinylpyrrolidone (PVP): As excipient from conventional to controlled delivery systems with a spotlight on COVID-19 inhibition. *J. Drug Delivery Sci. Technol.* **2020**, *60*, 102046.

(40) Franco, P.; De Marco, I. The Use of Poly(N-vinyl pyrrolidone) in the Delivery of Drugs: A Review. *Polymers* **2020**, *12* (5), 1114.

(41) Afzal, O.; Altamimi, A. S. A.; Nadeem, M. S.; Alzarea, S. I.; Almalki, W. H.; Tariq, A.; Mubeen, B.; Murtaza, B. N.; Iftikhar, S.; Riaz, N.; Kazmi, I. Nanoparticles in Drug Delivery: From History to Therapeutic Applications. *Nanomaterials* **2022**, *12* (24), 4494.

(42) Azam, A.; Ahmed, A. S.; Oves, M.; Khan, M. S.; Memic, A. Size-dependent antimicrobial properties of CuO nanoparticles against Gram-positive and -negative bacterial strains. *Int. J. Nanomed.* **2012**, *7*, 3527−3535.

(43) Venkateswarlu, K.; Thakur, H.; Babu, T. N. B. Fabrication of extended release tablets of pramipexole: in-vitro studies. *Pharm. Methods* **2017**, *8* (2), 115−120.

(44) Rakesh, S. S. S.; Anbazhagan, D. S.; Rao, M. B.; Sreekanth, J. Design and Evaluation of Extended Release Tablets of Pramipexole dihydrochloride monohydrate. *Int. J. Pharm. Sci. Rev. Res.* **2015**, *30* (1), 361−366.

(45) Nethravathi, P. C.; Pavan Kumar, M.; Suresh, D.; Lingaraju, K.; Rajanaika, H.; Nagabhushana, H.; Sharma, S. Tinospora cordifolia mediated facile green synthesis of cupric oxide nanoparticles and their photocatalytic, antioxidant and antibacterial properties. *Mater. Sci. Semicond. Process.* **2015**, *33*, 81−88.

(46) Ning, H.; Zhou, H.; Ren, J.; Zhou, G.; Yang, N.; Wang, Z.; Yuan, C.; Tian, Z.; Chen, J.; Shen, L.; Zheng, H.; Zhao, Y.; Wang, H.; Liu, W.; Liu, Z. Zishen pingchan granules combined with pramipexole in the improvement of depressive symptoms in Parkinson's disease: a prospective, multicenter, randomized, double-blind, controlled clinical study. *J. Transl. Med.* **2022**, *20* (1), 357.

(47) Oguro, H.; Kadota, K.; Ishihara, M.; Okada, K.; Yamaguchi, S. Efficacy of pramipexole for treatment of apathy in Parkinson's disease. *Int. J. Clin. Med.* **2014**, *5*, 885.

(48) Li, T.; Zou, S.; Zhang, Z.; Liu, M.; Liang, Z. Efficacy of pramipexole on quality of life in patients with Parkinson's disease: a systematic review and meta-analysis. *BMC Neurol.* **2022**, *22* (1), 320.

(49) Chernoloz, O.; El Mansari, M.; Blier, P. Long-term administration of the dopamine D3/2 receptor agonist pramipexole increases dopamine and serotonin neurotransmission in the male rat forebrain. *J. Psychiatry Neurosci.* **2012**, *37* (2), 113−121.

(50) Pramod Kumar, P.; Harish Prashanth, K. Diet with Low Molecular Weight Chitosan exerts neuromodulation in Rotenone induced Drosophila model of Parkinson's disease. *Food Chem. Toxicol.* **2020**, *146*, 111860.

(51) Lawana, V.; Cannon, J. R. Rotenone neurotoxicity: Relevance to Parkinson's disease. *Advances in Neurotoxicology*; Elsevier, 2020; Vol. 4, pp 209−254.

(52) Sian, J.; Dexter, D. T.; Lees, A. J.; Daniel, S.; Agid, Y.; Javoy-Agid, F.; Jenner, P.; Marsden, C. D. Alterations in glutathione levels in Parkinson's disease and other neurodegenerative disorders affecting basal ganglia. *Ann. Neurol.* **1994**, *36* (3), 348−355.

(53) Raj, R.; Wairkar, S.; Sridhar, V.; Gaud, R. Pramipexole dihydrochloride loaded chitosan nanoparticles for nose to brain delivery: Development, characterization and in vivo anti-Parkinson activity. *Int. J. Biol. Macromol.* **2018**, *109*, 27−35.

(54) Sherer, T. B.; Kim, J.-H.; Betarbet, R.; Greenamyre, J. T. Subcutaneous Rotenone Exposure Causes Highly Selective Dopaminergic Degeneration and α-Synuclein Aggregation. *Exp. Neurol.* **2003**, *179* (1), 9−16.

(55) Abolaji, A. O.; Fasae, K. D.; Iwezor, C. E.; Aschner, M.; Farombi, E. O. Curcumin attenuates copper-induced oxidative stress and neurotoxicity in Drosophila melanogaster. *Toxicol. Rep.* **2020**, *7*, 261−268.

(56) Abolaji, A. O.; Ajala, V. O.; Adigun, J. O.; Adedara, I. A.; Kinyi, H. W.; Farombi, E. O. Protective role of resveratrol, a natural polyphenol, in sodium fluoride-induced toxicity in Drosophila melanogaster. *Exp. Biol. Med.* **2019**, *244* (18), 1688−1694.

(57) Oyebode, O. T.; Abolaji, A. O.; Oluwadare, J. O.; Adedara, A. O.; Olorunsogo, O. O. Apigenin ameliorates D-galactose-induced lifespan shortening effects via antioxidative activity and inhibition of

mitochondrial-dependent apoptosis in Drosophila melanogaster. *J. Funct.Foodss* **2020**, *69*, 103957.

(58) Singh, M. P.; Himalian, R.; Shabir, S.; Obaid, A. A.; Alamri, A. S.; Galanakis, C. M.; Singh, S. K.; Vamanu, E. Protection of Phytoextracts against Rotenone-Induced Organismal Toxicities in Drosophila melanogaster via the Attenuation of ROS Generation. *Appl. Sci.* **2022**, *12* (19), 9822.

(59) Somasundaram, I.; Yadav, B.; Kumar, S. S. Formulation of PLGA Polymeric Nanosuspension containing Pramipexole Dihydrochloride for improved treatment of Parkinson's Diseases. *Res. J. Pharm. Technol.* **2016**, *9* (7), 810−816.

(60) Blakeman, D. P.; Ryan, T. P.; Jolly, R. A.; Petry, T. W. Diquat-dependent protein carbonyl formation: Identification of lipid-dependent and lipid-independent pathways. *Biochem. Pharmacol.* **1995**, *50* (7), 929−935.

(61) Dimock, A.; Siciliano, P.; McIlwraith, C. Evidence supporting an increased presence of reactive oxygen species in the diseased equine joint. *Equine Vet. J.* **2000**, *32* (5), 439−443.

(62) Siddique, Y. H.; Naz, F.; Khan, W.; Jyoti, S.; Raj Singh, B.; Naqvi, A. H. Effect of pramipexole alginate nanodispersion (PAND) on the transgenic Drosophila expressing human alpha synuclein in the brain. *J. Appl. Biomed.* **2018**, *16* (2), 111−119.

(63) Nahar, B.; Chaity, S. B.; Gafur, M.; Hossain, M. Z. Synthesis of Spherical Copper Oxide Nanoparticles by Chemical Precipitation Method and Investigation of Their Photocatalytic and Antibacterial Activities. *J. Nanomater.* **2023**, *2023*, 1−10.

(64) Phiwdang, K.; Suphankij, S.; Mekprasart, W.; Pecharapa, W. Synthesis of CuO nanoparticles by precipitation method using different precursors. *Energy Proc.* **2013**, *34*, 740−745.

(65) Saisri, B.; Anjaneyulu, V.; Kumar, G. V. DESIGN AND CHARATERIZATION OF PRAMIPEXOLE DIHYDROCHLORIDE NANOPARTICLES. *J. Innovat. Dev. Pharmaceut. Tech. Sci.* **2021**, *4* (11), 10.

(66) Somasundaram, I.; Sindhu, K. Formulation of Polymeric Nanosuspension Containing Pramipexole Dihydrochloride and Hesperidin for Improved Treatment of Parkinson's Diseases. *Asian J. Pharm. Clin. Res.* **2018**, *11*, 133−140.

(67) Pahuja, R.; Seth, K.; Shukla, A.; Shukla, R. K.; Bhatnagar, P.; Chauhan, L. K. S.; Saxena, P. N.; Arun, J.; Chaudhari, B. P.; Patel, D. K.; et al. Correction to trans-blood brain barrier delivery of dopamine-loaded nanoparticles reverses functional deficits in Parkinsonian Rats. *ACS Nano* **2019**, *13* (7), 8490.

(68) Tort, S.; Han, D.; Steckl, A. J. Self-inflating floating nanofiber membranes for controlled drug delivery. *Int. J. Pharm.* **2020**, *579*, 119164.

(69) Bahari Javan, N.; Jafary Omid, N.; Moosavi Hasab, N.; Rezaie Shirmard, L.; Rafiee-Tehrani, M.; Dorkoosh, F. Preparation, statistical optimization and in vitro evaluation of pramipexole prolonged delivery system based on poly (3-hydroxybutyrate-co-3-hydroxyvalerate) nanoparticles. *J. Drug Delivery Sci. Technol.* **2018**, *44*, 82−90.

(70) Papadimitriou, S.; Bikiaris, D.; Avgoustakis, K.; Karavas, E.; Georgarakis, M. Chitosan nanoparticles loaded with dorzolamide and pramipexole. *Carbohydr. Polym.* **2008**, *73* (1), 44−54.

(71) Sudati, J. H.; Vieira, F. A.; Pavin, S. S.; Dias, G. R.; Seeger, R. L.; Golombieski, R.; Athayde, M. L.; Soares, F. A.; Rocha, J. B.; Barbosa, N. V. Valeriana officinalis attenuates the rotenone-induced toxicity in Drosophila melanogaster. *Neurotoxicology* **2013**, *37*, 118−126.

(72) Fernandes, E. J.; Poetini, M. R.; Barrientos, M. S.; Bortolotto, V. C.; Araujo, S. M.; Santos Musachio, E. A.; De Carvalho, A. S.; Leimann, F. V.; Goncalves, O. H.; Ramborger, B. P.; Roehrs, R.; Prigol, M.; Guerra, G. P. Exposure to lutein-loaded nanoparticles attenuates Parkinson's model-induced damage in Drosophila melanogaster: Restoration of dopaminergic and cholinergic system and oxidative stress indicators. *Chem. Biol. Interact.* **2021**, *340*, 109431.

(73) Singh, M. P.; Himalian, R.; Shabir, S.; Obaid, A. A.; Alamri, A. S.; Galanakis, C. M.; Singh, S. K.; Vamanu, E. Protection of Phytoextracts against Rotenone-Induced Organismal Toxicities in

Drosophila melanogaster via the Attenuation of ROS Generation. *Appl. Sci.* **2022**, *12* (19), 9822.

(74) Feany, M. B.; Bender, W. W. A Drosophila model of Parkinson's disease. *Nature* **2000**, *404* (6776), 394−398.

(75) Bradford, M. M. A rapid and sensitive method for quantitation of microgram quantities of protein utilizing the principle of protein-dye binding. *Anal. Biochem.* **1976**, *72*, 248−254.

(76) Carvajal-Oliveros, A.; Domínguez-Baleón, C.; Zárate, R. V.; Campusano, J. M.; Narváez-Padilla, V.; Reynaud, E. Nicotine suppresses Parkinson's disease like phenotypes induced by Synphi-lin-1 overexpression in Drosophila melanogaster by increasing tyrosine hydroxylase and dopamine levels. *Sci. Rep.* **2021**, *11* (1), 9579.

(77) Maheswari, D. U.; Anand, T.; Manu, T. M.; Khanum, F.; Sharma, R. K. Motion sickness induces physiological and neuronal alterations in a mouse model. *Int. J. Res. Pharm. Sci.* **2019**, *10*, 1650−1659.

(78) Das, S. K.; Patel, B.; Patri, M. Neurotoxic Effect of Benzo[a]pyrene and Its Possible Association with 6-Hydroxydopamine Induced Neurobehavioral Changes during Early Adolescence Period in Rats. *J. Toxicol.* **2016**, *2016*, 1−7.

(79) Bianchini, M. C.; Gularte, C. O. A.; Nogara, P. A.; Krum, B. N.; Gayer, M. C.; Bridi, J. C.; Roos, D. H.; Roehrs, R.; Fachinetto, R.; Pinton, S.; et al. Thimerosal inhibits Drosophila melanogaster tyrosine hydroxylase (Dm TyrH) leading to changes in dopamine levels and impaired motor behavior: implications for neurotoxicity. *Metallomics* **2019**, *11* (2), 362−374.

(80) Habig, W. H.; Jakoby, W. B. [51] Assays for differentiation of glutathione S-Transferases. *Methods in Enzymology*; Elsevier, 1981; Vol. *77*, pp 398−405.

(81) Jollow, D.; Mitchell, J.; Zampaglione, N. a.; Gillette, J. Bromobenzene-induced liver necrosis. Protective role of glutathione and evidence for 3, 4-bromobenzene oxide as the hepatotoxic metabolite. *Pharmacology* **1974**, *11* (3), 151−169.

(82) Spirlandeli, A. L.; Deminice, R.; Jordao, A. Plasma malondialdehyde as biomarker of lipid peroxidation: effects of acute exercise. *Int. J. Sports Med.* **2014**, *35*, 14−18.

(83) Siddique, Y. H.; Mujtaba, S. F.; Faisal, M.; Jyoti, S.; Naz, F. The effect of Bacopa monnieri leaf extract on dietary supplementation in transgenic Drosophila model of Parkinson's disease. *Eur. J. Integr. Med.* **2014**, *6* (5), 571−580.